

Discovery of an X-ray Synchrotron Nebula Associated with the Radio Pulsar PSR B1853+01 in the Supernova Remnant W44

Ilana M. Harrus¹, John P. Hughes²

Harvard-Smithsonian Center for Astrophysics

60 Garden Street, Cambridge, MA 02138

and David J. Helfand

Astronomy Department, Columbia University

538 West 120th Street, New York, NY 10027

Received 24th February 1996; accepted 5th April 1996

To appear in the June 20th issue of the *Astrophysical Journal Letters*.

¹Department of Physics, Columbia University, New York, NY 10027

²E-mail: jph@cfa.harvard.edu

ABSTRACT

We report the detection using data from the *Advanced Satellite for Cosmology and Astrophysics* (*ASCA*) of a hard X-ray source in the vicinity of the radio pulsar PSR B1853+01, which is located within the supernova remnant (SNR) W44. PSR B1853+01, a 267 ms pulsar, has to date been detected only in the radio band. Previous observations at soft X-ray energies (e.g., with *ROSAT* HRI) have failed to detect any significant X-ray emission (pulsed or unpulsed) from the pulsar. In addition, no high energy emission ($\gtrsim 4$ keV) has been detected previously from W44.

Over the 0.5–4.0 keV band, the *ASCA* data show soft thermal emission from W44, with a morphology very similar to that observed earlier by *Einstein* and *ROSAT*. In the high-energy band (4.0–9.5 keV), the SNR is, for the most part, invisible, although a source coincident with the position of PSR B1853+01 is evident. The observed *ASCA* spectra are consistent with a power-law origin (photon index ~ 2.3) for the X-ray emission from this source at a flux level (flux density $\sim 0.5 \mu\text{Jy}$ at 1 keV) consistent with previous upper limits. The maximum allowed size for the source is determined directly from the *ASCA* data ($< 5'$), while the minimum size is derived from the nondetection of a point source in the *ROSAT* HRI data ($\gtrsim 30''$). Timing analysis of the hard X-ray source failed to detect pulsations at the pulsar's period. Based on these lines of evidence, we conclude that the new hard source in W44 represents an X-ray synchrotron nebula associated with PSR B1853+01, rather than the beamed output of the pulsar itself. This discovery adds W44 to the small group of previously known plerionic SNRs. This nebula lies at the low end of, but is consistent with, the correlation between X-ray luminosity and pulsar spin-down energy loss found for such objects, lending further support to our interpretation.

Subject headings: ISM: individual (W44)– pulsars: individual (PSR B1853+01)
– radiation mechanisms: nonthermal – supernova remnants – X-rays: ISM

1. Introduction

The radio pulsar PSR B1853+01 was discovered by Wolszczan, Cordes, & Dewey (1991) inside the radio shell of the supernova remnant W44. The estimated distances to the pulsar and the supernova remnant (SNR) are both on the order of 3 kpc, and the age deduced from the spin-down of the pulsar (20,000 yrs) is compatible with the dynamical age of the remnant inferred from X-ray observations (Harrus & Hughes 1994; Harrus et al. 1996). Previous work has failed to detect X-ray emission from PSR B1853+01 in any of the expected forms: pulsed or unpulsed emission from the pulsar itself, or nonthermal emission from an associated synchrotron nebula. No high energy tail was seen in the *Ginga* spectrum, leading to a 3σ upper limit of 3.6×10^{-12} ergs cm $^{-2}$ s $^{-1}$ for the 2–10 keV flux of a Crablike power-law component ($dN/dE \sim E^{-2.1}$) from W44 (Harrus & Hughes 1994; Harrus et al. 1996). Although there was a report of a high-energy component to the X-ray spectrum of W44 from *EXOSAT* data (Rho et al. 1994), an earlier analysis (Jones, Smith, & Angellini 1993) had already indicated that this component arose from contamination of the data by particle background events and that, in fact, the SNR was undetected above 5 keV. Moreover neither a point source nor pulsed emission was seen at the pulsar position in the *ROSAT* PSPC observation in the soft X-ray band (Rho et al. 1994). In this Letter, we report on the discovery of the anticipated nonthermal X-ray emission from the vicinity of PSR B1853+01 using spectral, imaging, and timing observations from *the Advanced Satellite for Cosmology and Astrophysics (ASCA)* (Tanaka, Inoue, & Holt 1994).

2. Analysis

ASCA conducted two observations of W44. The first, carried out on 1994 April 22, had a nominal pointing direction of 18^h56^m24^s, 1°16′58″ (J2000). In anticipation of a search for pulsed X-ray emission from PSR B1853+01 (period \simeq 267ms), we rearranged Gas Imaging Spectrometer (GIS) telemetry bits in order to record photon arrival times more accurately

at the expense of pulse-height (PH) rise-time information. This modification increased the GIS time resolution to 15.625 ms (medium telemetry rate mode) and 1.95 ms (high telemetry rate mode) from their nominal values of 500 and 62.5 ms, respectively. Data from the GIS were rejected during times when the satellite was traversing regions of low geomagnetic rigidity (≤ 7) and when the Earth elevation angle was $\leq 10^\circ$. The data were also masked spatially to remove the bright ring of background around the edge of the detector as well as the calibration source events. The Solid-State Imaging Spectrometer (SIS) time resolution of 8 s and 16 s, in the 2-CCD and 4-CCD modes used in the observation was clearly too low to detect pulsed emission from PSR B1853+01. The SIS screening criteria used in extracting spectral information were very similar to the ones applied to the GIS: minimum Earth elevation angle of 10° and a minimum rigidity of 6. Because of the possibility for contamination in the SIS of fluorescence lines of oxygen from the Earth's atmosphere, data selection was done on the bright-Earth angle, and only data above 40° (20°) for the SIS0 (SIS1) were retained. Finally, only events with CCD grades 0, 2, 3, or 4 were used in further analysis.

For the second observation, carried out on 1994 September 10, the nominal pointing direction was changed to $18^{\text{h}}55^{\text{m}}55^{\text{s}}$, $1^\circ 28' 18''$ and the GIS telemetry bit assignments were set to their nominal values. Consequently, the pulsar region was not included in the field of view (FOV) of the SIS detectors and the time resolution of the GIS data was inadequate for the pulsar search study, although the GIS imaging data are included in this study. The total exposure time on W44 was approximately 39 ks (GIS) and 48 ks (SIS) summing the two pointings.

Below, we present spatial, spectral, and timing analysis of these data, which reveal an X-ray synchrotron nebula associated with the pulsar.

2.1. Spatial Analysis

We generated exposure-corrected, background-subtracted merged images of the GIS and SIS data in selected spectral bands. Background was determined from the weighted average of several nominally blank fields from high Galactic latitude observations with data selection criteria matched to those used for the W44 data. Exposure maps were generated from the off-axis effective-area calibrations, weighted by the appropriate observation time. Events from regions of the merged exposure map with less than 10% of the maximum exposure were ignored. Merged images of the source data, background, and exposure were smoothed with a Gaussian of $\sigma = 30''$ for the low-energy band (0.5–4.0 keV) and $\sigma = 90''$ for the high-energy band (4.0–9.5 keV). We subtracted smoothed background maps from the data maps and divided by the corresponding exposure map. Figure 1 shows the results obtained for the two detectors in each of the two energy bands. The low-energy band shows the soft thermal X-ray emission from W44, with a morphology very similar to that observed before by *Einstein* (Smith et al. 1985) and *ROSAT* (Rho et al. 1994). In the high-energy band, however, the SNR is not visible and only a few unresolved sources appear. The most significant of these is coincident with the position of the radio pulsar. In the 4.0–9.5 keV band, this source is detected with a signal-to-noise ratio of ~ 9 , and at higher energies (6.0–9.5 keV), the signal-to-noise ratio is ~ 4 . The other significant source, located about $10'$ northwest of the pulsar in the GIS image, has a signal-to-noise ratio of ~ 5.0 (4.0–6.0 keV); it is not detected above 6 keV. We suggest that this second source arises from temperature variation within the SNR itself and that we are seeing the tail of the emission from a higher temperature parcel of shocked plasma. (Note that the apparent difference in relative intensities of these sources as observed by the SIS and GIS is most likely a result of the different spectral resolution of the two detectors. The SIS, because of its better spectral resolution, can discriminate better against out-of-band photons, e.g., those below 4 keV, than can the GIS.) We will be addressing temperature variations in W44 in greater detail in future work.

In the GIS (considering the sum of the GIS2 and GIS3 detectors), the number of photons at energies greater than 4 keV within a 5' radius centered on the pulsar position is 310 ± 21 counts (for an exposure time 12,670 s) after subtracting a background image derived from high Galactic latitude observations. Elsewhere in the FOV of the GIS outside the remnant boundaries, a similar size region at a similar off-axis angle (9' for the test region compared to 6' for the pulsar region) in the same band yields roughly 98 ± 13 counts. This excess of events in an apparently source-free portion of the image is due to the Galactic plane X-ray background emission, as we show in our spectral analysis below. In the SIS, the region selected for the pulsar analysis is smaller (radius of 3') in order not to cross individual chip boundaries. The number of events seen at high energy (again summing the two detectors SIS0 and SIS1) is 150 ± 14 , compared with 37 ± 8 found in a source-free region elsewhere in the FOV of the SIS. In Table 1, we have summarized the positions of the radio pulsar (Wolszczan 1995) and the associated X-ray source, as measured by the two *ASCA* detectors. The errors given in the table include both statistical and systematic uncertainties. The pulsar's position is indicated by a cross in Figure 1.

TABLE I
POSITION OF PSR B1853+01
AND ASSOCIATED X-RAY SOURCE

	R.A.(J2000)	Decl.(J2000)
Radio^a	$18^{\text{h}}56^{\text{m}}10.79^{\text{s}} \pm 0.04^{\text{s}}$	$1^{\circ}13'28'' \pm 2''$
X-ray:GIS	$18^{\text{h}}56^{\text{m}}10.0^{\text{s}} \pm 1.5^{\text{s}}$	$1^{\circ}13'17'' \pm 40''$
X-ray:SIS	$18^{\text{h}}56^{\text{m}}12.6^{\text{s}} \pm 1^{\text{s}}$	$1^{\circ}12'34'' \pm 30''$

^a Wolszczan 1995

A recent high-resolution radio map of W44 shows an elongated diffuse feature with a flat spectral index (-0.12 ± 0.04) extending north from the pulsar's position (Frail et al. 1996). The peak of this emission is centered at approximately $18^{\text{h}}56^{\text{m}}11^{\text{s}}$, $1^{\circ}13'24''$ and it is extended over an elliptical region $\sim 1'$ in right ascension and $\sim 2'$ in declination. We note that the position of the new hard X-ray source is consistent with that of the pulsar, while it is marginally inconsistent with the peak position of the diffuse radio nebula to the north.

2.2. Spectral analysis

Our previous work on W44 (Harrus & Hughes 1994; Harrus et al. 1996) has shown that the remnant’s global integrated X-ray emission can be described adequately using a simple nonequilibrium ionization plasma model (Hughes & Singh 1994), characterized by a temperature $kT = (0.88 \pm 0.14)$ keV, an ionization timescale $n_e t = (2.0_{-0.7}^{+4.3}) \times 10^{11}$ cm⁻³ s, and a column density $N_H = (1.0_{-0.2}^{+0.6}) \times 10^{22}$ atoms cm⁻². The errors are quoted at the 90% confidence level. In this model, the ionization timescale characterizes deviations from ionization equilibrium; the larger the value, the closer the plasma is to equilibrium, which occurs at a value $\sim 3 \times 10^{12}$ cm⁻³ s. For simplicity, and in view of the large value of the ionization timescale, we have approximated the SNR spectrum with a single-temperature Raymond & Smith (1977; version 9.00 in XSPEC) thermal plasma model. Line-of-sight absorption by the interstellar medium is included using the cross sections from Morrison & McCammon (1983).

The Galactic plane is a strong source of diffuse X-ray emission that can be modeled well in the 2–10 keV band by a thermal bremsstrahlung continuum with a temperature $kT \sim 7$ keV, and a narrow emission line from highly ionized iron ($E \sim 6.8$ keV), with an equivalent width ~ 0.6 keV (Yamauchi 1991). Previous observations of roughly this area of the sky by *Tenma* (Koyama 1989) and *Ginga* (Yamauchi 1991) suggest a surface brightness in the range $(0.56\text{--}2.26) \times 10^{-7}$ ergs cm⁻² s⁻¹ sr⁻¹ for the plane emission (2–10 keV band). These instruments, however, had large fields of view ($\sim 3^\circ$ FWHM for *Tenma*, and $1^\circ \times 2^\circ$ FWHM for *Ginga*), and it is not known how structured the plane emission is on smaller angular scales ($\sim 5'$). In order to normalize the intensity of the plane emission for the *ASCA* analysis, we selected a “control” region of the same size as the pulsar region, located elsewhere in the field of view, making sure that the control and pulsar regions were disjoint. Our procedure entailed determining the intensity of the Galactic plane emission (for a fixed set of spectral parameters) from the control region, and then applying that

normalization and set of spectral parameters to the X-ray spectrum extracted from the pulsar region.

Figure 2 shows the results of the fit and the residuals associated with these models. In this analysis, as well as in the timing analysis discussed below, we have used data from the first observation taken in medium-bit-rate mode. Using the intensity of the Galactic plane emission deduced from the fit of the control region, we study the data extracted from a circular region of radius $5'$ ($3'$) in the GIS (SIS), centered on the radio pulsar position. First, we fit the data in the pulsar region with a Raymond & Smith (1977) plasma model, plus the Galactic plane background model, and find a χ^2 of 622 (567) and a reduced χ^2 of 1.8 (4.0), for the GIS (SIS) data. Then we fix the parameters at their best-fit values and include an additional power-law component fitted to the band above 3 keV only. The $\Delta\chi^2$ (computed over the whole range of energy) of these fits is greater than 30 for the GIS and greater than 50 for the SIS (a reduction significant at more than the 99% confidence level); the power-law index is $2.3_{-0.9}^{+1.1}$, and its normalization is $0.7_{-0.5}^{+2.3}\times 10^{-3}$ photons cm^{-2} s^{-1} keV^{-1} at 1 keV in the GIS ($0.6_{-0.5}^{+2.1}\times 10^{-3}$ photons cm^{-2} s^{-1} keV^{-1} at 1 keV in the SIS). The errors on the slope of the power-law combine the statistical error (which dominates) and the uncertainties in the Galactic background model used. We varied the temperature of the background bremsstrahlung continuum between 6 and 8 keV, and we also varied the normalization of the model at a fixed temperature. The uncertainties are then combined in quadrature. The associated remnant temperature is 0.5 ± 0.2 keV, and the column density is $(1.82\pm 0.05)\times 10^{22}$ atoms cm^{-2} . We show the results for the GIS only in Figure 3; GIS 2 and 3 have been merged for display purposes only.

2.3. Timing analysis

We have carried out a timing analysis on events recorded in the two GIS with a time resolution of 15.6 ms. We select only the 453 events coming from the same region as the one used in the spectral analysis and having an energy larger than 4 keV (to discriminate against photons coming from the SNR itself). Folding the data with the known radio timing parameters of $P = 0.26743520599(6)$ s and \dot{P} of $(208.482 \pm 0.006) \times 10^{-15}$ s s $^{-1}$ (Wolszczan 1995), we find no significant modulation at the 3σ level.

One limitation of such a folding method is its dependence on bin size: the data are binned according to the phase difference between the corrected arrival time and the period. Considering the small number of photons available, we have also performed a Z_n test (Buccheri et al. 1983) summing harmonics with $n \leq 4$. The Z_n test is free of the bias of the bin size chosen in the folding method and is sensitive to a range of pulse shapes depending on the order of the test (larger n implies sensitivity to narrower pulse shapes). We have used simulated data to put an upper limit of 10% on the pulsed fraction for the emission above 4 keV. This limit depends only weakly on the order of the Z_n test performed.

3. Discussions and Conclusions

We have presented the results of morphological and spectral studies of the contribution from PSR B1853+01 to the X-ray emission of the SNR W44. High-energy emission in both the GIS and the SIS is found at the position of the pulsar; the spectra from both instruments require a power-law component to model the observed emission. A lower limit to the spatial extent of the emission region can be derived from the average *ROSAT* HRI surface brightness around the pulsar position, which, after subtraction of the nominal HRI background, is $\sim 4 \times 10^{-3}$ counts arcmin $^{-2}$ s $^{-1}$. Based on our spectral analysis, we expect an HRI count rate from the power-law component of $(2.0\text{--}3.5) \times 10^{-3}$ counts s $^{-1}$. This

translates into a minimum angular size of $\sim 30''$. Using the known distance to the SNR, we deduce an emission volume of $2.78 D_{3\text{kpc}}^3 \theta^3 \text{ pc}^3$, where $D_{3\text{kpc}}$ is the distance to the SNR in units of 3 kpc, and θ is the angular size of the nebula expressed in arcminutes. An upper limit on the source size can be obtained from the *ASCA* data. We have simulated images with Gaussian source profiles of various widths and convolved each with the PSF of the mirror and the detector, weighted according to the spectrum from the pulsar region. We then cross-correlated the simulated images with the GIS image and deduced an upper limit to the source radius of $\sim 5'$.

The inferred unabsorbed flux from the power-law component extrapolated to the *ROSAT* energy band (0.4–2.0 keV) is $1.9_{-1.4}^{+9.1} \times 10^{-12} \text{ ergs cm}^{-2} \text{ s}^{-1}$; the value of $1.2 \pm 0.3 \times 10^{-12} \text{ ergs cm}^{-2} \text{ s}^{-1}$, measured for the 2–10 keV band flux, is in agreement with the upper limit of $3.6 \times 10^{-12} \text{ ergs cm}^{-2} \text{ s}^{-1}$ obtained using the *Ginga* spectrum (Harrus & Hughes 1994; Harrus et al. 1996). The unabsorbed X-ray luminosity in the *Einstein* band (0.2–4.0 keV) is $(4_{-3}^{+30}) \times 10^{33} D_{3\text{kpc}}^2 \text{ ergs s}^{-1}$, which should be compared to the luminosity predicted by the empirical \dot{E}/L_X relation (Seward & Wang 1988) of $7.7 \times 10^{32} \text{ ergs s}^{-1}$.

Frail et al. (1996) present new radio data on the nebula surrounding PSR B1853+01 and, using the *Ginga* upper limit, construct a spectrum covering 10 decades in frequency from the radio to the X-ray bands. From these data, the equipartition value of the nebular magnetic field, B_n , and the energy in relativistic electrons, E_e , can be estimated by assuming that the break in the spectrum between the radio and X-ray regimes is due to synchrotron losses (Pacholczyk 1970, p 169). Our *ASCA* measurements of the X-ray flux and spectral index of the nebula allow better determination of the break frequency, that is, the frequency where the extrapolated X-ray and radio power-law spectra intersect. The best-fit spectral values indicate a value of $\nu_B \sim 2 \times 10^{13} \text{ Hz}$. (Note that the break frequency of the Crab Nebula is $\sim 10^{13} \text{ Hz}$.) We find for the nebular magnetic field $B_n \simeq 70 \mu\text{G} (V_R/3.1 \times 10^{55} \text{ cm}^3)^{-2/7}$ (using the estimated volume of the radio nebula, V_R , and the luminosity integrated from 10^7 Hz to ν_B which is $2.3 \times 10^{34} \text{ ergs s}^{-1}$) and for the

energy in electrons $E_e \simeq 10^{46}$ ergs $(B_n/70 \mu\text{G})^{-3/2}$, values that are consistent with other plerionic SNRs of comparable luminosity.

The lifetime of the electrons giving rise to the radio emission, $\sim 20,000$ yr, is of the same order as the age of the SNR and pulsar, while the electrons giving rise to the X-ray emission are quite short-lived, ~ 120 yr. Consequently, the X-ray synchrotron nebula should be significantly smaller than the radio nebula and should be located close to the pulsar, as indicated by our *ASCA* data. In particular, given the parameters derived above, we expect essentially no nonthermal X-ray emission from the bright diffuse radio-emitting nebula north of the pulsar, since the pulsar would have traversed this region over 2000 years ago, given the projected distance and the inferred transverse motion, 375 km s^{-1} , of PSR B1853+01 (Frail et al. 1996). A follow-up X-ray observation of the pulsar region with high spatial resolution should be able to confirm this conjecture and, in addition, provide a number of new constraints on the energetics of the synchrotron nebula. In any event, the *ASCA* data presented here provide strong evidence for the oldest synchrotron nebula yet detected, a result that should aid considerably in our attempts to understand the interaction of pulsar relativistic winds with their environments.

We thank Alex Wolszczan for providing an accurate position and a recent ephemeris for PSR B1853+01 and we thank E. Churazov, M. Gilfanov and A. Finoguenov for allowing us to use their software for merging *ASCA* images. Pat Slane, Olaf Vancura, Paul Callanan, Didier Barret, Rick Harnden, and Fred Seward are acknowledged for their helpful comments and discussions. This research was partially supported by NASA Grant NAG 5-2605 and the Smithsonian Institution, through the Smithsonian Predoctoral Fellowship program. This is contribution 595 of the Columbia Astrophysics Laboratory.

REFERENCES

- Buccheri, R. et al. 1983, *A & A*, 128, 245
- Frail, D. A., Giacani, E. B., Goss, W. M., & Dubner, G. 1996, *ApJL*, in press
- Harrus, I. M., & Hughes, J. P. 1994, *BAAS*, 26, 1429
- Harrus, I. M., Hughes, J. P., Singh, K. P., Koyama, K., & Asaoka, I. 1996, *ApJ*, in preparation
- Hughes, J. P., & Singh, K. P. 1994, *ApJ*, 422, 126
- Jones, L. R., Smith, A., & Angellini, L. 1993, *MNRAS*, 265, 631
- Koyama, K. 1989, *PASJ*, 41, 665
- Morrison, R., & McCammon, D. 1983, *ApJ*, 270, 119
- Pacholczyk, A. G. 1970, *Radio Astrophysics* (San Francisco: Freeman)
- Raymond, J. C., & Smith, B. W. 1977, *ApJS*, 35, 419
- Rho, J. H., Petre, R., Schlegel, E. M., & Hester, J. 1994, *ApJ*, 430, 757
- Seward, F. D., & Wang, Z. R. 1988, *ApJ*, 332, 199
- Smith, A., Jones, L. R., Watson, M. G., Willingale, R., Wood, N., & Seward, F. D. 1985, *MNRAS*, 217, 99
- Tanaka, Y., Inoue, H., & Holt, S. S. 1994, *PASJ*, 46, L37
- Wolszczan, A. 1995, private communication
- Wolszczan, A., Cordes, J. M., & Dewey, R. J. 1991, *ApJ*, 372, L99
- Yamauchi, S. 1991, Ph.D. thesis, Nagoya Univ

This manuscript was prepared with the AAS L^AT_EX macros v4.0.

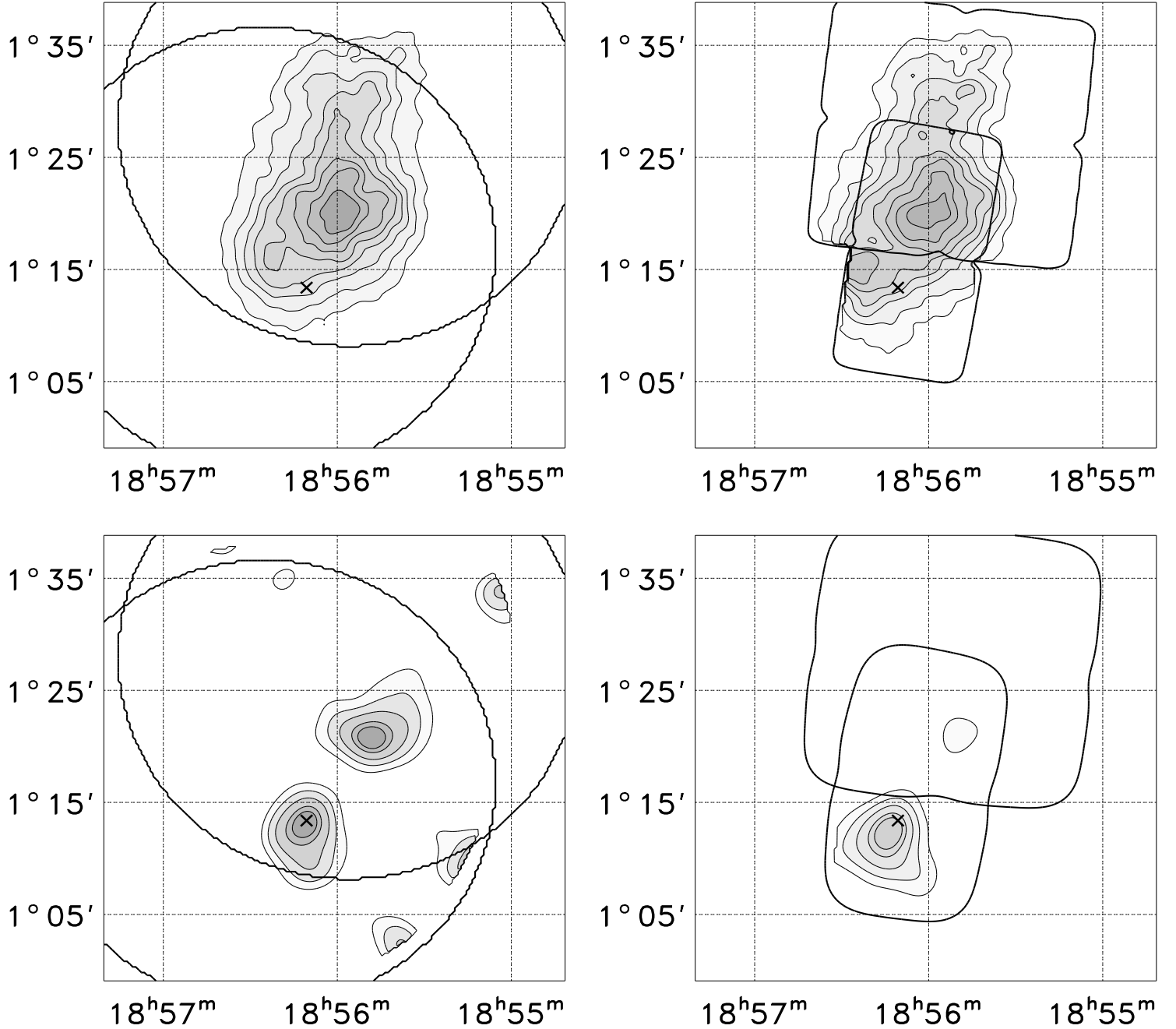


Figure 1: GIS and SIS images, background subtracted and exposure corrected. The images in the low-energy band (*upper pair*: 0.5–4.0 keV) have been smoothed with a Gaussian of $\sigma = 30''$, while the images in the high-energy band (*lower pair*: 4.0–9.5 keV) have been smoothed with a Gaussian of $\sigma = 90''$. The exposure maps have been truncated below 10% of the maximum exposure in the energy band considered. We show schematically the fields of view of the two pointings (*bold lines*). The position of the pulsar is indicated by a cross on each of the four panels. Contour values in the upper panels are linearly spaced from 10% to 90% of the peak surface brightness in each map. For the GIS (*left panel*) the peak map value is $1.50 \times 10^{-2} \text{ counts s}^{-1} \text{ arcmin}^{-2}$, while for the SIS (*right panel*) it is $1.95 \times 10^{-2} \text{ counts s}^{-1} \text{ arcmin}^{-2}$. Contour levels in the lower panels correspond to values of 60%, 70%, 80%, 90%, and 95% of the peak. The peak surface brightness values here are $2.56 \times 10^{-4} \text{ counts s}^{-1} \text{ arcmin}^{-2}$ (GIS) and $2.76 \times 10^{-4} \text{ counts s}^{-1} \text{ arcmin}^{-2}$ (SIS).

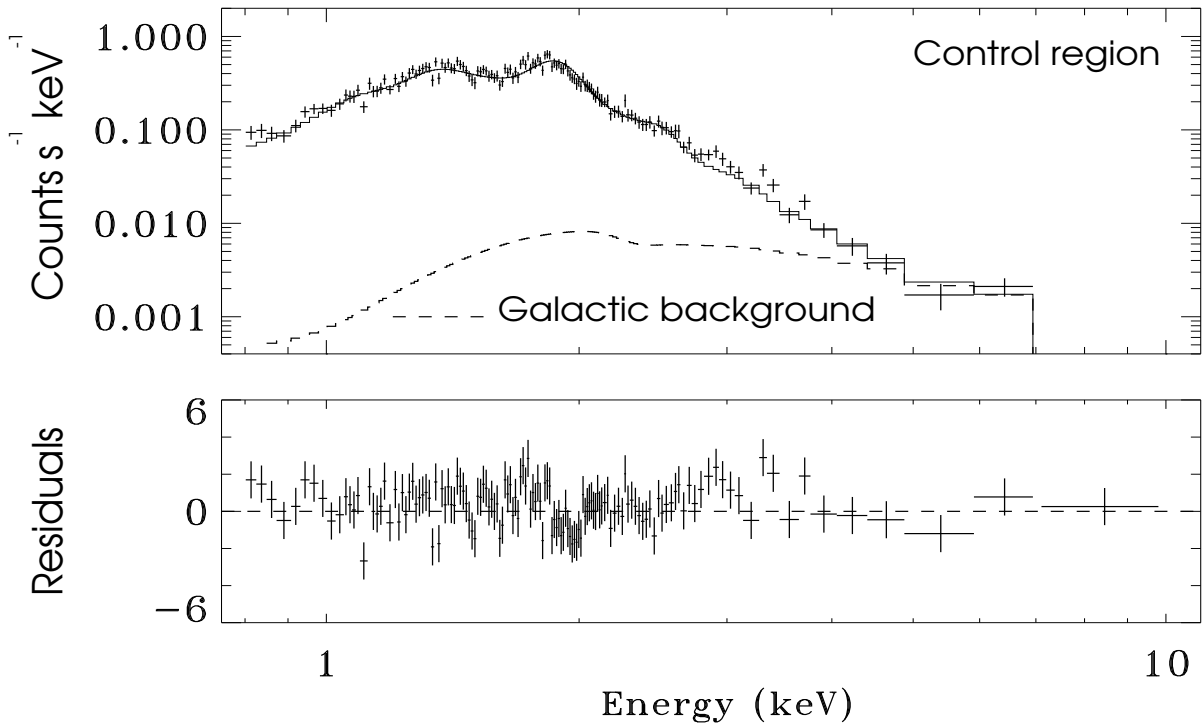


Figure 2: Fit of the GIS spectrum extracted from the control region. The dotted line represents the contribution of the Galactic plane modeled by a bremsstrahlung at 7 keV and a Gaussian iron line at 6.8 keV, with a sigma of 50 eV and an equivalent width 0.6 keV (see Yamauchi 1991).

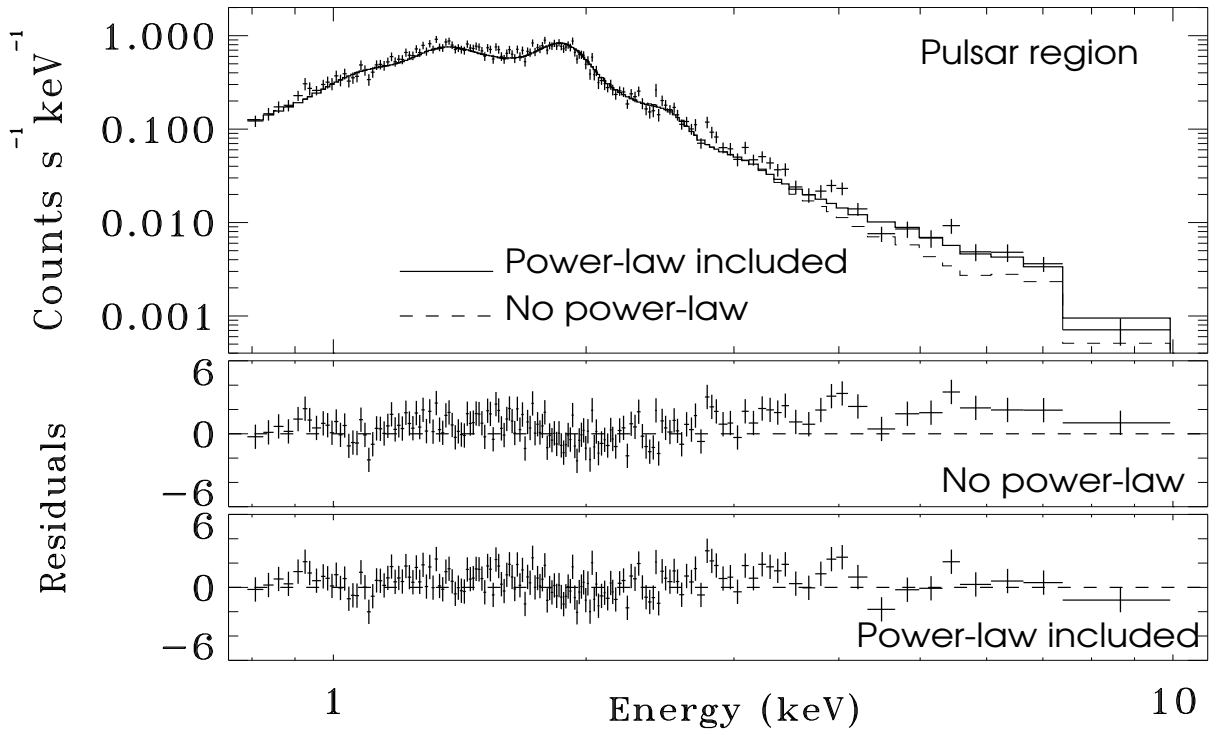


Figure 3: The GIS spectrum extracted from a 5' radius region centered at the radio pulsar position. Fits with (solid) and without (dashed) a power-law component are shown; this fit without the power-law component shows a clear excess in all residuals above 3 keV.